Desalination and Water Treatment
www.deswater.com
doi: 10.5004/dwt.2020.26316

206 (2020) 263–272
December

Novel graphene oxide based adsorbents for removing water pollutants Pb^{2+}, Cd^{2+}, Mn^{2+}, and Mg^{2+} ions

Yan Zhang[a,b,*], Feng Liang[a,b], Pingge Dian[b], Zhan Chen[b]

[a]*Henan Province Key Laboratory of Water Pollution Control and Rehabilitation Technology, Henan University of Urban Construction, Pingdingshan, Henan 467036, China, emails: zhangyan696@163.com (Y. Zhang), liangfeng@hncj.edu.cn (F. Liang)*
[b]*Department of Environmental and Municipal Engineering, Henan University of Urban Construction, Pingdingshan 467036, China, emails: louis0375@163.com (P. Dian), cz1343028511@163.com (Z. Chen)*

Received 30 January 2020; Accepted 27 June 2020

ABSTRACT

Novel adsorbent is prepared by modifying graphene oxide/sodium alginate with disodium ethylenediaminetetraacetate (SGE). Benefiting from the network-alike structure, and the abundant hydroxyl and amino groups, the removal of SGE for Pb^{2+}, Cd^{2+}, Mn^{2+}, and Mg^{2+} ions from water is effective and fast at neutral pH values. The adsorption equilibrium of SGE for Pb^{2+}, Cd^{2+}, Mn^{2+}, and Mg^{2+} ions can be well-modeled with the Langmuir isotherm. The adsorption processes of Pb^{2+}, Cd^{2+}, Mn^{2+}, and Mg^{2+} ions onto SGE are shown to follow the kinetics of pseudo-second-order reactions. The maximum adsorption capacities for Pb^{2+}, Cd^{2+}, Mn^{2+}, and Mg^{2+} ions are 121.2, 117.1, 56.7, and 41.8 mg/g at 298 K, respectively. The desorption and regeneration experiments show that the respective adsorption capabilities for Pb^{2+}, Cd^{2+}, Mn^{2+}, and Mg^{2+} are approximately 92.8%, 91.1%, 89%, and 85.7% after the 5th cycle. These results demonstrate that SGE composite is a promising adsorbent for the treatment of wastewater heavy metal ions.

Keywords: Sodium alginate composites; Adsorption; Pb^{2+}; Cd^{2+}; Mn^{2+}; Mg^{2+}; Wastewater

1. Introduction

Heavy metal ions such as Pb^{2+} and Cd^{2+} ions are commonly used in a number of industrial processes, and the accumulation of these ions in nature poses serious environmental problems worldwide. Though Mn^{2+} and Mg^{2+} ions are necessary micronutrient elements for plants and human beings, they could also induce damages to human health if their amounts exceed a certain threshold. According to the WHO regulation, the permissible limits of the metal concentrations in drinking-water samples are 0.05 mg/L for Pb, 0.003 mg/L for Cd, and 0.5 mg/L for Mn [1]. Therefore, it is essential to effectively purify the metal-ions containing industrial effluents so that their concentrations fulfill the international safety standard. Nowadays many strategies have been developed to remove metal ions in fluid, including flocculation–coagulation [2], electro-chemical precipitation [3], cyanide treatment [4], ion exchange [5], and adsorption [6,7]. Adsorption is the most widely used method because of its high efficiency, easy-handling, and low cost. Especially, carbon-based adsorbent such as activated carbon [4,8,9], carbon nanotubes [10], and graphene [11], have been applied to remove organic and inorganic pollutants in water treatment [12].

Graphene oxide (GO) is a two-dimensional material, which possesses abundant adsorption sites and high surface area [9,13,14]. GO possesses a corrugated carbon sheet with over half of the carbon atoms are functionalized with hydroxyl and epoxy groups. Its edges are partially occupied by hydroxyl, carboxyl, ketone, ester, and even lactol groups [13,14]. Due to a large amount of available functional groups and π-electron system [15], GO can be easily

* Corresponding author.

chemical-modified; and hence offers abundant binding sites for the adsorption of metal ions. Its practical application is, however, limited since GO has high hydrophilicity, which makes it difficult to be separated from the treated water.

To fully use the special structural properties of GO, and at the same time minimize the disadvantages from its hydrophilicity, other strategies can be combined. For example, sodium alginate (SA), a kind of polyanion electrolyte including many carboxylic acids, has been widely used for water treatment because of its non-toxicity, biocompatibility, and high viscosity [16,17]. Its three-dimensional network structure can be easily prepared by cross-linking with sodium alginate and calcium. In addition, disodium ethylenediaminetetraacetate (EDTA) is a well-known heavy metal ion chelating agent through its four carboxyl and two amino groups. Therefore novel adsorbents based on the above components could be promising for enhancing the adsorption of metal ions in water [18].

In this paper, a simple synthesis route is developed and a novel type of adsorbent named SA/GO/EDTA (SGE) can be obtained. The structural property of this new adsorbent is characterized using scanning electron microscopy (SEM). The removal of the SGE foam for Pb^{2+}, Cd^{2+}, Mn^{2+}, and Mg^{2+} in aqueous solutions at varying pH values, initial ions concentrations and contact times are systematically compared. The adsorption kinetics and mechanisms are analyzed using different models. In the end, the regeneration of the adsorbents is investigated.

2. Experimental

2.1. Materials

Graphite flakes are acquired from Sigma-Aldrich (St. Louis, USA). EDTA, $Pb(NO_3)_2$, $CdCl_2$, $MnCl_2$, and $Mg(NO_3)_2$ are purchased from Sinopharm Chemical Reagent Co., Ltd., (Shanghai, China). All the other chemicals used in this study are analytical grade. De-ionized water is used for the preparation of all required solutions.

2.2. Preparation of GO and sodium alginate composites

GO is synthesized from natural graphite powders according to a modified Hummers method [19]. Firstly, graphite flakes (1.5 g) are added to concentrated H_2SO_4 (180 mL) and H_3PO_4 (20 mL) solution under mild agitation at ice temperature. $KMnO_4$ (9 g) is then slowly added to the suspension under stirring. The rate of addition is carefully controlled to keep the reaction temperature below 25°C. Afterwards, the temperature is increased to 50°C and maintained for 12 h under continuous stirring. De-ionized water (500 mL) is then slowly added to the mixture and the reaction temperature is controlled at 98°C for 2 h. The mixture solution is subsequently treated with H_2O_2 (30 mL, 30 wt.%). This mixture is repeatedly centrifuged and washed several times with a 10% HCl aqueous solution to remove the metal ions. Finally, the mixture is filtered and washed with de-ionized water until its pH value reaches about 7. The resulted GO is freeze-dried for 24 h. For the following chemical synthesis, GO is dispersed in de-ionized water in an ultrasonic bath for 2 h to obtain a colloidal solution of 3 g/L.

The SGE materials are synthesized using the reported method [20]. SA (0.4 g) and EDTA (0.1 g) are dissolved completely in a 10 mL GO solution using a magnetic stirrer for 4 h. The solution is set for 12 h to remove the air bubbles. Afterward, it is frozen in an ultra-low temperature freezer at –80° (DW-HL540, Zhongke Meiling low-temperature Technology Co., Ltd., Hefei, China) for 1 h. Subsequently, it is dried in a vacuum freeze drying machine (SCIENTZ-10, Xinzhi Biotechnology Co., Ltd., Ningbo, China). The resulted foam-alike composite is soaked in a 1% $CaCl_2$ solution for 1 h for cross-linking. Finally, the SGE foam is washed with de-ionized water to remove the residual calcium chloride and is dried at 50°C afterward.

2.3. Characterization

The morphology of the SGE foams is characterized by FEI Quanta 450 SEM is made in USA. Fourier transform infrared (FT-IR) spectra are obtained using a Nicolet iS10 spectrometer of Thermo Fisher Scientific is made in USA. Inductively coupled plasma optical emission spectrometer (Optima7000, PE Company, USA) is used to determine concentrations of the heavy metal ions.

2.4. Experimental methods

The synthesized SGE materials, cut into thin strips, are put into the mixed aqueous solutions at a concentration of 0.5 g/L. The concentration of Pb^{2+}, Cd^{2+}, Mn^{2+}, and Mg^{2+} ions is 10 mg/L, respectively. To facilitate the adsorption of heavy metal ions, the mixture solution is stirred for 3 h in a temperature-controlled water bath shaker. Afterward, the concentrations of the Pb^{2+}, Cd^{2+}, Mn^{2+}, and Mg^{2+} ions in the liquid phase are analyzed using an inductively coupled plasma optical emission spectrometer. The amount of adsorption and the removal rate is calculated as the following.

To calculate the amount of adsorption at the equilibrium, Eq. (1) is used.

$$q_e = \frac{\left(c_0 - c_e\right)}{m} \times V \tag{1}$$

To calculate the removal rate, Eq. (2) is used:

$$R\% = \frac{\left(c_0 - c_e\right)}{c_0} \times 100\% \tag{2}$$

where q_e is the equilibrium adsorption (mg/g), V the solution volume (L), m the mass of the adsorbent (g), c_0 the initial concentration of Pb^{2+}, Cd^{2+}, Mn^{2+}, and Mg^{2+} ions (mg/L), c_e the concentration of Pb^{2+}, Cd^{2+}, Mn^{2+}, and Mg^{2+} ions at the adsorption equilibrium (mg/L), and R the removal rate (%).

3. Results and discussion

3.1. Characterization of material morphology

The surface and fracture edges of the SGE foam are characterized using SEM, and the results are shown in Figs. 1a and b. The surface of SGE clearly reveals abundant porous structure with varying pore sizes. The fracture edges image (Fig. 1b) reveals well-ordered and vertically-arranged channel-like morphology. Such a kind

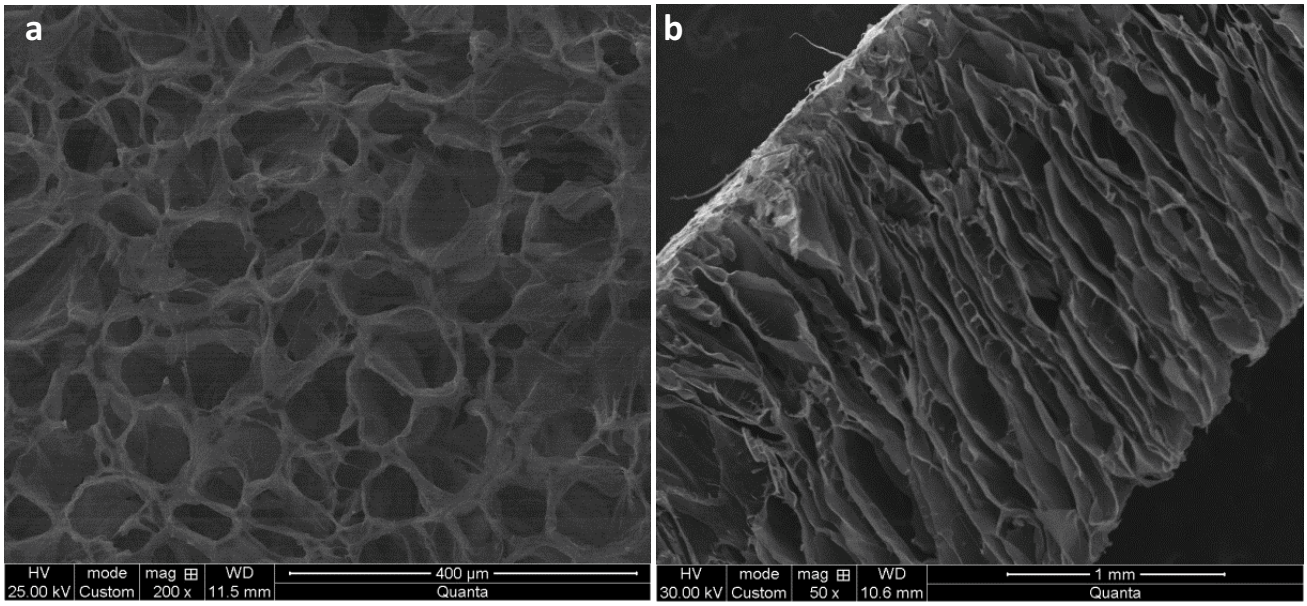

Fig. 1. SEM images are taken from the surface (a) and the cross-section (b) of SGE foam.

of morphology is probably caused by two reasons. Firstly, the EDTA molecules and GO layers are wrapped with SA, forming an interconnected network with Ca^{2+} ions through interactions such as hydrogen-bonds, and van de Waals forces [21,22]. The material property such as mechanical strength and resilience is improved because of excellent toughness of GO sheets and high elasticity of SA chains [23–25]. Secondly, the formation of ice crystals from the bottom to the top leads to a honeycomb-structured after lyophilization of solution [26]. The GO layers are relatively ordered alignment along the growth direction of the ice crystals. After the sublimation of ice crystal, the channel-alike morphology is left in the foam. The particular "riband bridges" structure of the SGE foam is dense which indicates an excellent tensile strength [27]. The possible self-assembly procedure mechanism of the SGE is illustrated in Scheme 1. With *in situ* crosslinking processes, the edges of GO sheets interact with adjacent EDTA molecules and SA chains. Hence the GO sheets and EDTA are able to be immobilized in the SA matrix [23].

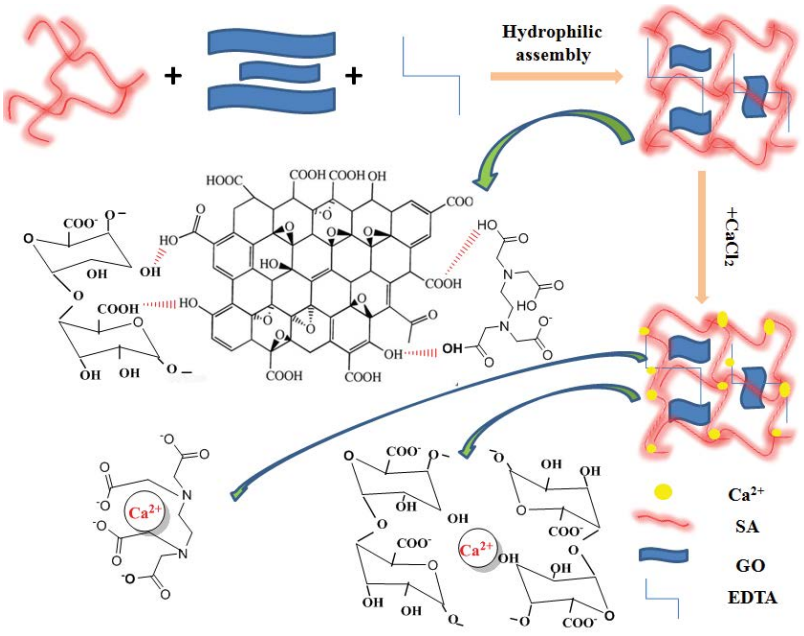

Scheme 1. Schematic illustration of the synthesis process and adsorption mechanism of the SGE.

Fig. 2 shows the FT-IR spectra of GO, SA, EDTA, and SGE foam. For the native GO, the IR peaks at 3,555; 1,715; 1,604; and 1,325 cm^{-1} are assigned to the OH stretching vibration, C=O stretching vibration of the carboxylic group, C=C stretching in the C–O–C group, and –OH in the alcohol group, respectively [28]. For SA, the IR peak at 3,566 cm^{-1} is due to the OH stretching vibration. Moreover, the peaks at 1,592 and 1,402 cm^{-1} are attributed to the symmetric and asymmetric COO^- stretching vibration of the carboxylate salt group, and the peak located at 1,028 cm^{-1} is the stretching vibration of the C–O–C groups [29]. For EDTA, the IR peaks at 3,022 and 2,948 cm^{-1} are the symmetric and asymmetric $–CH_2$ stretching vibration of the linear paraffin. The peaks at 1,623 and 1,400 cm^{-1} are the symmetric and asymmetric COO^- stretching vibration of the carboxylate salt group [30]. The FTIR spectrum of SGE foam reveals the characteristic peaks of SA chains, EDTA chains, and GO sheets. The two peaks at 2,928 and 2,846 cm^{-1} from the symmetric and asymmetric $–CH_2$ stretching vibration of the EDTA chains can be observed, which suggests that EDTA has been linked into the SGE foam. Molecular interactions via hydrogen bonding often occur when organic substances have certain functional groups, such as –COOH, –OH, and $–NH_2$ [31]. In the molecular structure of EDTA there are six coordination atoms including two nitrogen atoms and four carboxyl oxygen atoms. They could provide lone-pair electrons to form hydrogen bonds, such as O–H···O or O–H···N, with the hydroxyl-rich GO sheets and SA chains. Furthermore, the OH stretching vibration which appears at 3,555 cm^{-1} in GO and 3,556 cm^{-1} in SA, is broadened, strengthened, and shifts to 3,270 cm^{-1} in SGE. This phenomenon indicates that SA, EDTA, and GO in the SGE foam are interconnected via strong hydrogen-bonding interactions. In the IR spectrum of SGE foam, it is evident that when SA, EDTA, and GO cross-linked with Ca^{2+}, the symmetric COO^- peak shifts to a higher wavenumber (from 1,402 to 1,412 cm^{-1}) and the asymmetric COO^- peak shifts to lower wavenumber (from 1,592 to 1,584 cm^{-1}). This phenomenon has been assigned to cross-linking via strong interactions between the carboxylate group and the multivalent cation [25,32].

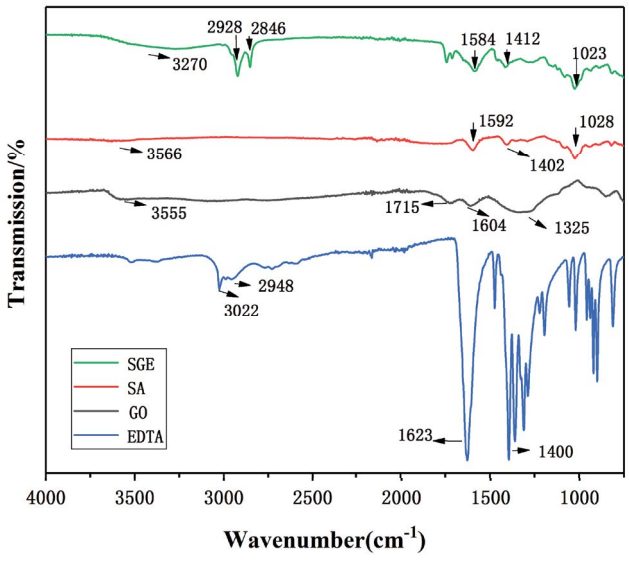

Fig. 2. FT-IR spectra of GO, SA, EDTA, and SGE foam.

3.2. Effect of solution pH values

The solution pH values, varied from 3 to 7, are investigated to determine the removal rates of Pb^{2+}, Cd^{2+}, Mn^{2+}, and Mg^{2+} ions by the SGE foam. As shown in Fig. 3, the removal rates increase with the increase of pH value from 3 to 6. The reason could be that the carboxyl and hydroxyl groups of the SGE foam are protonated at the lower pH values, which weakens the electrostatic attraction with the cations [33]. The amount of protons decreases at higher pH values. Therefore, the competitive adsorption induced by protons with the SGE foam decreases, which in turn increases the possibilities that metal ions Pb^{2+}, Cd^{2+}, Mn^{2+}, and Mg^{2+} to adsorb onto the SGE foam. On the other hand, the pH has an important effect on the dissociation equilibrium of EDTA. Depending on the solution pH values, various species like H_6Y^{2+}, H_5Y^+, H_4Y^-, H_3Y^-, H_2Y^{2-}, HY^{3-}, and Y^{4-} (Y = EDTA) exist in the aqueous solution [34]. It has been reported that the chelating ability of EDTA with the Pb^{2+}, Cd^{2+}, Mn^{2+}, and Mg^{2+} ions increases with the increasing pH values [35]. Considering that $Pb(OH)_2$ will be formed at pH values higher than 7.5, a solution pH value of 6 is chosen for the following experiments [36,37].

3.3. Effect of metal ions concentration

As shown in Fig. 4, the relationship between adsorption capacity of SGE foam and initial ions concentrations is plotted. With the increase of initial concentration of Pb^{2+}, Cd^{2+}, Mn^{2+}, and Mg^{2+} ions, the threshold of their adsorption equilibrium increases gradually. This tendency slows down when the initial concentrations reach 50 mg/L for Mn^{2+}, and Mg^{2+} ions, and 70 mg/L for Pb^{2+}, Cd^{2+} ions. The phenomenon

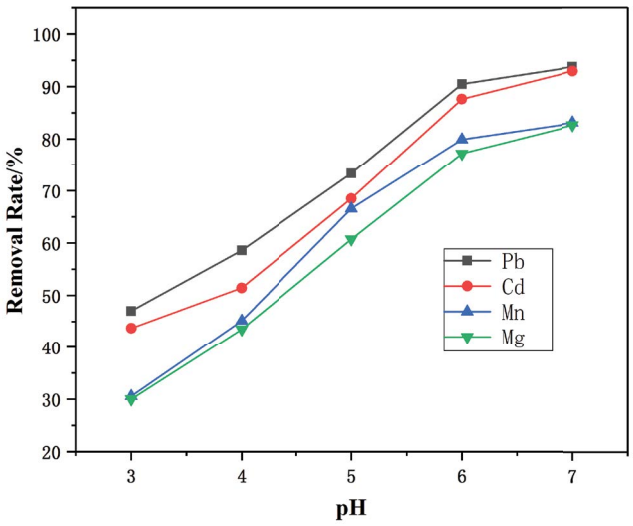

Fig. 3. Dependence of ion removal rate on the solution pH value. The initial concentrations of Pb^{2+}, Cd^{2+}, Mn^{2+}, and Mg^{2+} ions in the mixed solution are 10 mg/L, respectively. Adsorbent dose is 0.5 g/L, T = 293 K.

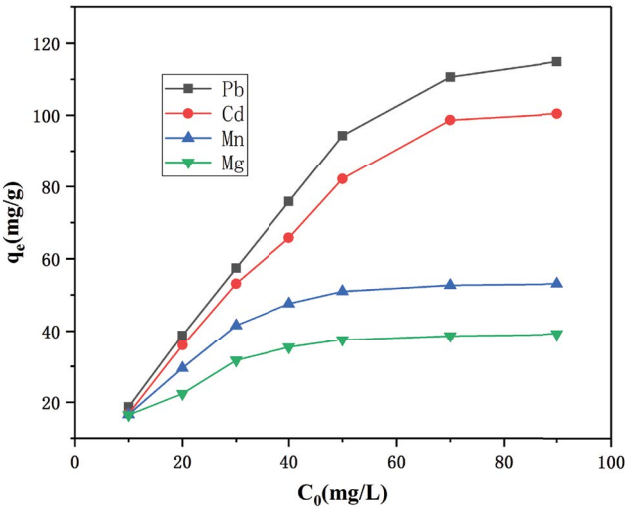

Fig. 4. Dependence of amount of adsorption at equilibrium on the initial metal ion concentration. The initial concentrations of Pb^{2+}, Cd^{2+}, Mn^{2+}, and Mg^{2+} ions in the mixed solution vary between 10 and 90 mg/L, respectively. Adsorbent dose is 0.5 g/L, pH = 6, and T = 293 K.

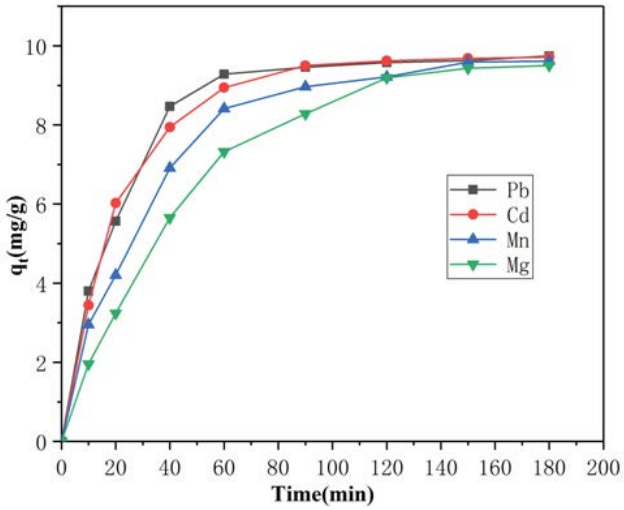

Fig. 5. Dependence of amount of adsorption on the contact time. The initial concentrations of Pb^{2+}, Cd^{2+}, Mn^{2+}, and Mg^{2+} ions in the mixed solution are 10 mg/L, respectively. Adsorbent dose is 0.5 g/L, pH = 6, and T = 293 K.

indicates that the adsorptions of these four metal ions by SGE foam are saturated. It also shows that the adsorption equilibrium of Mn^{2+} and Mg^{2+} ions are reached earlier on the SGE foam than it is for the Pb^{2+} and Cd^{2+} ions.

3.4. Effect of contact time

The equilibrium time is studied as one of the most essential parameters for water treatment. Fig. 5 shows that the adsorption rates toward the four metal ions onto SGE foam increase dramatically in the initial 60 min. The phenomenon could be attributed to two reasons. First, at the beginning, abundant vacant sites and surface area are available for the adsorption of these ions. Second, the strong attractive forces between the SGE foam and heavy metal ions facilitate the fast diffusion of heavy metal ions into the inter-space of the foam [38–40]. The adsorption rate reaches equilibrium in about 120 min., indicating that the available vacant adsorption sites decrease gradually and the diffusion of metal ions into the inter-space of SGE foams takes much more time [41,42].

3.5. Adsorption kinetics

In order to investigate the adsorption kinetics, the pseudo-first-order kinetic model, and the pseudo-second-order kinetic model [43] are used to fit the experimental results. The pseudo-first-order kinetic rate equation is expressed as:

$$\log\left(q_e - q_t\right) = \log q_e - \frac{k_1}{2.303}t \tag{3}$$

where q_e and q_t (mg/g) are the adsorption capacities at equilibrium time and time t (min), respectively. k_1 (1/min) is the rate constant of pseudo-first-order. The values of k_1 and q_e can be obtained from the slope and intercept of $\log(q_e - q_t)$ vs. t, respectively. The pseudo-first-order kinetic model describes a physical absorption mechanism.

The pseudo-second-order equation is expressed as follows:

$$\frac{t}{q_t} = \frac{1}{k_2 q_e^2} + \frac{t}{q_e} \tag{4}$$

where k_2 (g/(mg·min)) is the rate constant of the pseudo-second-order reaction. The values of q_e and k_2 can be obtained from the slope and intercept of t/q_t vs. t, respectively. The pseudo-second-order kinetic model assumes that the adsorption mechanism is a chemical process.

The adsorption kinetics of Pb^{2+}, Cd^{2+}, Mn^{2+}, and Mg^{2+} ions onto SGE foam are shown in Fig. 6, and the kinetic model parameters calculated using Eqs. (3) and (4) are listed in Table 1. It is shown that the correlation coefficients (R^2) for the pseudo-second-order kinetic model are larger than those using the pseudo-first-order kinetic model, suggesting that the adsorption of Pb^{2+}, Cd^{2+}, Mn^{2+}, and Mg^{2+} ions onto SGE foam fits the pseudo-second-order kinetic model better. So the rate-limiting step of Pb^{2+}, Cd^{2+}, Mn^{2+}, and Mg^{2+} ions onto SGE foam might be chemisorption process [37,44].

Furthermore, the intra-particle diffusion model is often used to describe the rate-control step in a material possessing porous structure, and its equation is presented as [45]:

$$q_t = k_i t^{1/2} \tag{5}$$

where C is the intercept and k_i is the intra-particle diffusion rate constant (g/(mg $\min^{1/2}$)).

The straight lines in Fig. 7 indicate that the fitting results follow the intra-particle diffusion model. The regressions of q_t vs. $t^{1/2}$ are shown to be linear. However, they don't pass through the "0" position, suggesting that though the

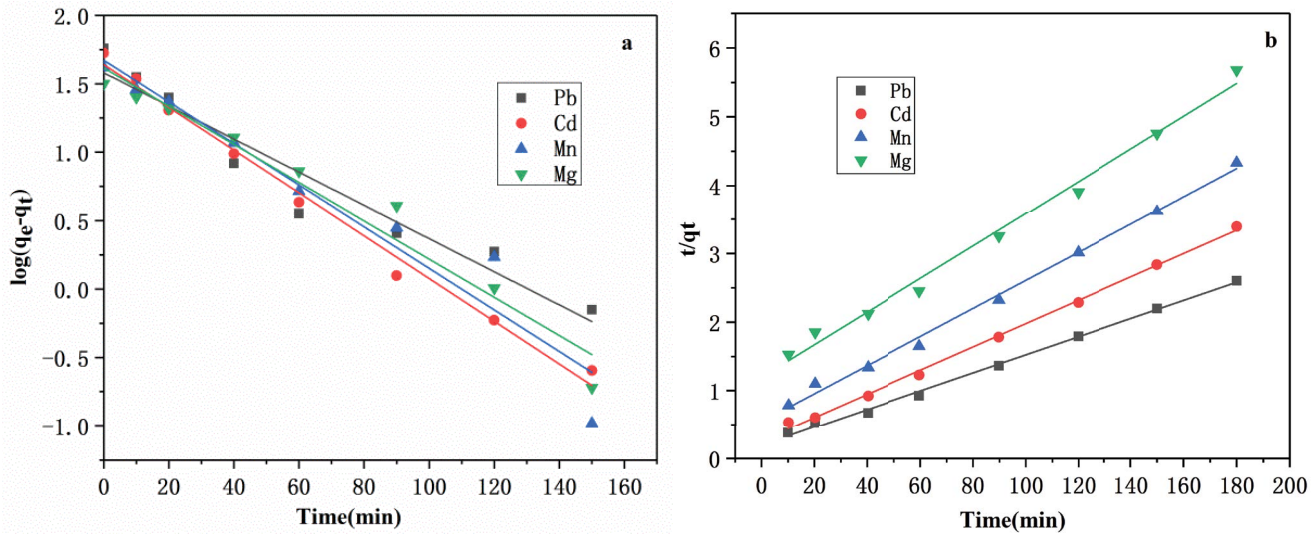

Fig. 6. Analyzing the adsorption mechanisms using pseudo-first-order (a) and pseudo-second-order (b) models. The initial concentrations of Pb^{2+}, Cd^{2+}, Mn^{2+}, and Mg^{2+} ions in the mixed solution are 30 mg/L, respectively. Adsorbent dose is 0.5 g/L, pH = 6, and T = 293 K.

Table 1
Kinetic model parameters for Pb^{2+}, Cd^{2+}, Mn^{2+}, and Mg^{2+} adsorption onto SGE foam

Metal ions	Pseudo-first-order kinetic		Pseudo-second-order kinetic		Partical diffusion model			
	k_1 (1/min)	R^2	k_2 (g/(mg·min))	R^2	k_{i1} (g/(mg·min$^{1/2}$))	R_1^2	k_{i2} (g/(mg·min$^{1/2}$))	R_2^2
Pb^{2+}	0.0279	0.92712	3.45×10^{-5}	0.99667	8.27	0.99722	0.633	0.98922
Cd^{2+}	0.036	0.98943	7.82×10^{-5}	0.99739	8.10	0.98773	0.705	0.81205
Mn^{2+}	0.035	0.92715	2.32×10^{-4}	0.99469	5.56	0.99322	0.942	0.95791
Mg^{2+}	0.0322	0.95752	6.80×10^{-4}	0.98963	4.17	0.99354	1.33	0.91623

adsorption process involves intra-particle diffusion, it is not the only rate-control step [46,47]. Indeed, two adsorption processes including external diffusion and intra-particle diffusion can be involved. In the beginning, the steep increase of q_t vs. $t^{1/2}$ is referred to as diffusion of ions through the solution to the internal space of the SGE foam. In the second step, the relationship of q_t vs. $t^{1/2}$ is rather flat, which is corresponding to the diffusion of metal ions inside the pore of the SGE foam [48].

In general, the adsorption performances of SGE foam toward the four ions decrease with the order of Pb^{2+}, Cd^{2+}, Mn^{2+}, and Mg^{2+}. The higher adsorption performance towards Pb^{2+} and Cd^{2+} ions could be due to their material-property dependent affinities with the adsorbents [49,50]. For example, the electronegativities of Pb^{2+}, Cd^{2+}, Mn^{2+}, and Mg^{2+} ions are 2.33, 1.69, 1.55, and 1.31, respectively. It has been reported that ions with large electronegativities are easier to form a stable complex with the oxygen-containing function groups via lone-pair electrons [51,52]. Indeed, the stability constants (lgK) of the EDTA complexes with the respective ions are 18.04 for Pb-EDTA, 16.46 for Cd-EDTA, 13.87 for Mn-EDTA, and 8.69 Mg-EDTA [53]. There are coordination reactions between Pb^{2+}, Cd^{2+}, Mn^{2+}, and Mg^{2+} ions and O and N atoms in EDTA. Moreover, the lgK of the EDTA complexes with Pb^{2+}, Cd^{2+}, and Mn^{2+} ions is bigger than that of Ca^{2+} (lgK = 10.69), there is ion exchange between the Ca in SGE foam and Pb^{2+}, Cd^{2+}, and Mn^{2+} ions in solution [54,55]. These factors are conducive to the competitive adsorption of the four ions by the adsorbent. Furthermore, the radii of the Pb^{2+}, Cd^{2+}, Mn^{2+}, and Mg^{2+} ions are 0.119, 0.095, 0.067, and 0.072 nm, respectively. The smaller the ion radius is, the easier the ion can diffuse into the porous foam to access the internal binding sites. This could be an additional reason for the different adsorption capacity of the SGE foam toward these four ions. Notably, the radii of Mn^{2+} ion is smaller than that of the Pb^{2+}, Cd^{2+}, and Mg^{2+} ions, which would in principle allow the Mn^{2+} ion to diffuse into the porous foam easier. However, the experimental results show that the adsorption performances of the Pb^{2+}, Cd^{2+}, and Mn^{2+} ions do not comply with the evolution of the ion radii. Therefore, the significant selective adsorption of Pb^{2+}, Cd^{2+}, Mn^{2+}, and Mg^{2+} ions should be the result of combination factors.

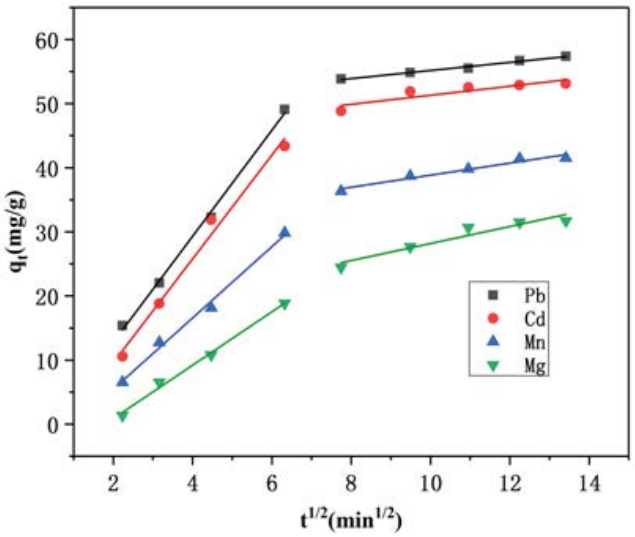

Fig. 7. Analyzing the dependence of q_t on $t^{1/2}$ using the intra-particle diffusion model. The straight lines are the fitting results. The initial concentrations of Pb^{2+}, Cd^{2+}, Mn^{2+}, and Mg^{2+} ions in the mixed solution are 30 mg/L, respectively. Adsorbent dose is 0.5 g/L, pH = 6, and T = 293 K.

3.6. Adsorption isotherms

Adsorption isotherm models are usually used to determine the mechanism of adsorption. Here, both Langmuir [56] and Freundlich [57] isotherms in the linear form are applied.

Langmuir model:

$$\frac{c_e}{q_e} = \frac{c_e}{q_m} + \frac{1}{q_m K_L} \tag{6}$$

Freundlich model:

$$\ln q_e = \ln K_F + \frac{1}{n}\ln c_e \tag{7}$$

where c_e is the equilibrium concentration (mg/L), q_e is the adsorption capacity at equilibrium (mg/g), q_m is the maximum amount of adsorbent (mg/g), K_L is the equilibrium adsorption constant (L/mg), K_F and n are Freundlich constants related to the adsorption capacity and adsorption intensity, respectively.

In order to obtain adsorption isotherms of Pb^{2+}, Cd^{2+}, Mn^{2+}, and Mg^{2+} ions onto SGE foam, the adsorptions of ions from 10 to 90 mg/L are studied in mixed solution, respectively. The isotherm plots (Fig. 8) and the related parameters (Table 2) show that the adsorption behaviors can be better fitted with the Langmuir models, where the R^2 values are generally higher than those with the Freundlich isotherms. This result suggests that the adsorption of four metals on SGE foam is on monolayer coverage. According to the Langmuir model, the maximum adsorption capacities of the foam are 121.2 mg/g (Pb^{2+}), 117.1 mg/g (Cd^{2+}), 56.7 mg/g (Mn^{2+}) and 41.8 mg/g (Mg^{2+}) at 293 K, respectively.

The excellent adsorption ability of the SGE foam can, therefore, be understood considering the following factors: (1) according to the result of SEM analysis, the SGE foam is three-dimensionally connected which has well-shaped porous surface and vertically-arranged channel-like cross-section. Such kind of structural properties provides a large amount of adsorption sites and sufficiently large volume for metal ions to enter the interlayer space of the adsorbent; (2) according to the FT-IR analysis, there are abundant oxygen-containing functional groups on the surface and interlayer of the SGE foam that can easily bind metal cations; (3) the de-localized π-electron systems of the GO sheet acts as the Lewis base, whilst the heavy metal

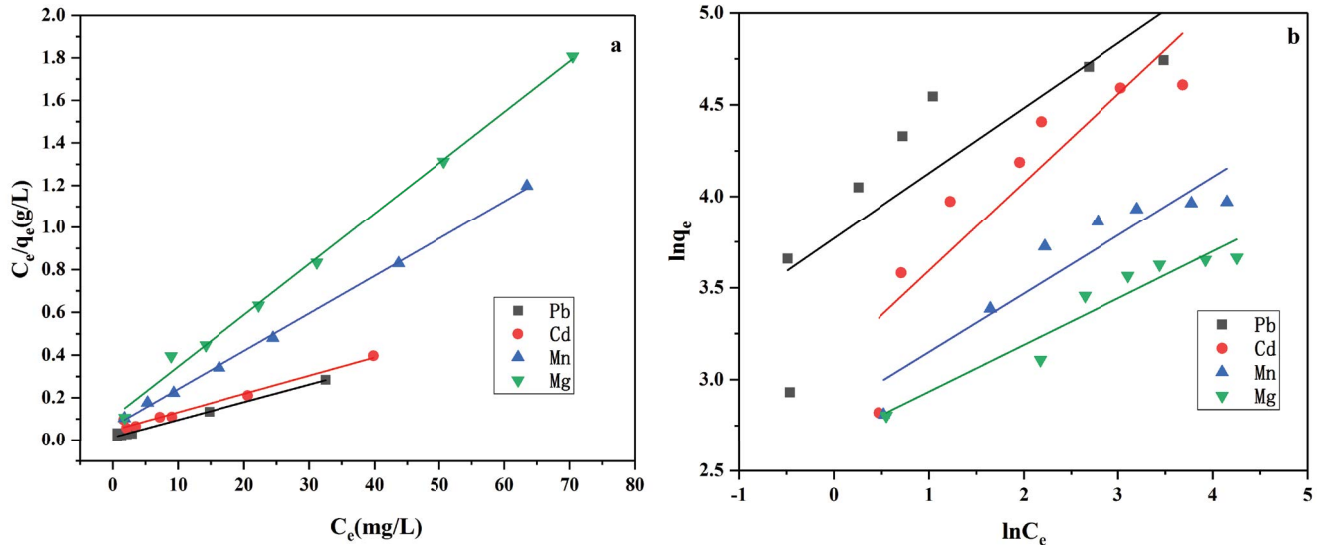

Fig. 8. Analyzing the adsorption mechanisms using Langmuir (a) and Freundlich (b) isotherms. The initial concentrations of Pb^{2+}, Cd^{2+}, Mn^{2+}, and Mg^{2+} ions in the mixed solution vary between 10 and 90 mg/L, respectively. Adsorbent dose is 0.5 g/L, pH = 6, and T = 293 K.

Table 2
Isothermal constants for Pb^{2+}, Cd^{2+}, Mn^{2+}, and Mg^{2+} adsorption onto SGE foam

Metal ions	Langmuir isotherms			Freundlich isotherms		
	K_L (L/mg)	q_m (mg/g)	R^2	K_F (L/mg)	$1/n$	R^2
Pb^{2+}	0.606	121.2	0.99479	43.299	0.35587	0.68502
Cd^{2+}	0.183	117.1	0.97795	22.2934	0.48439	0.79409
Mn^{2+}	0.269	56.7	0.99892	16.9101	0.3194	0.87537
Mg^{2+}	0.221	41.8	0.9959	14.5328	0.25541	0.9221

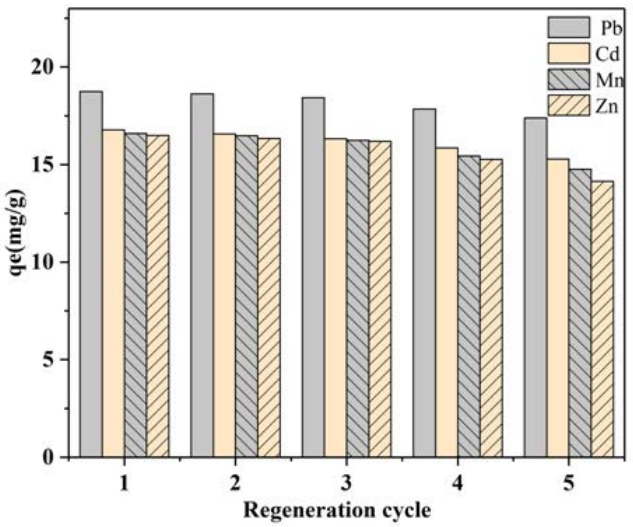

Fig. 9. Regeneration properties of the SGE foam. The initial concentrations of Pb^{2+}, Cd^{2+}, Mn^{2+}, and Mg^{2+} ions in the mixed solution are 10 mg/L, respectively. Adsorbent dose is 0.5 g/L, pH = 6, and T = 293 K.

ions can act as the Lewis acid. Hence, the delocalized π electron systems form electron donor-acceptor complexes with heavy metal ions through the Lewis acid-base interaction [48]; (4) possessing tertiary amines and carboxylate groups, EDTA is a prominent complexing agent with metal ion which can further enhance the adsorption capabilities toward Pb^{2+}, Cd^{2+}, Mn^{2+}, and Mg^{2+} ions [58].

3.7. Desorption and regeneration

The desorption and regeneration of the adsorbent are critical requirements for reducing the overall cost when applying absorbents for practical use. After the equilibrium condition is reached, the desorption experiment is conducted by adding 80 mg SGE into 160 mL mixed solution, which contains Pb^{2+}, Cd^{2+}, Mn^{2+}, and Mg^{2+} ions of 10 mg/L, respectively. After the adsorption process, the foam is collected and put into a solution of 0.2 mol/L glycine – HCl and shaked for 4 h. After the above processes, the resulted adsorbent is rinsed with de-ionized water for five times to remove the residual glycine – HCl and dried at 40°C afterwards. Then, the foam is used repeatedly in order to study the regeneration property of the adsorbent. The respective adsorption capabilities for Pb^{2+}, Cd^{2+}, Mn^{2+}, and Mg^{2+} are shown to be approximately 92.8%, 91.1%, 89%, and 85.7% after the fifth cycle (Fig. 9). The slight decrease is probably due to the loss of binding sites such as OH groups, COOH groups, and EDTA chains of SGE foam at each desorption step.

4. Conclusions

A novel adsorbent is synthesized by mixing SA, EDTA, and GO for the removal of metal ions. The SEM characterization shows that the compound possesses three-dimensional network structures and regular porous morphology with high mechanic strength. The pH value influences significantly the adsorption capabilities. The adsorption kinetics and isotherms are analyzed in detail, and the results show that the adsorption follows pseudo-second-order kinetics. The equilibrium data are fitted well with the Langmuir isotherm model. The maximum adsorption capacities of the foam for Pb^{2+}, Cd^{2+}, Mn^{2+}, and Mg^{2+} ions are 121.2, 117.1, 56.7, and 41.8 mg/g at 298 K, respectively. This outstanding removal performance is likely due to the synergy of physical adsorption as well as chemical adsorption processes. These results provide evidence for estimating and optimizing the removal of metal ions from wastewater by using SGE composites in the future.

Acknowledgments

The authors gratefully acknowledge the financial support provided by the Key Scientific Research Project Plan of Henan Higher Education Institutions (16A610007), the Scientific and Technological Key Projects in Henan Province (182102310847), and the Scientific Research Capability Upgrading Project in Henan University of Urban Construction (2017YY048).

References

[1] World Health Organization (WHO) Health Criteria Other Supporting Information, Guidelines for Drinking Water Quality, Vol. 2, 2nd ed., WHO, Geneva, 1996.
[2] A.J. Hargreaves, P. Vale, J. Whelan, L. Alibardi, C. Constantino, G. Dotro, E. Cartmell, P. Campo, Coagulation-flocculation process with metal salts, synthetic polymers and biopolymers for the removal of trace metals (Cu, Pb, Ni, Zn) from municipal wastewater, Clean Technol. Environ. Policy, 20 (2018) 393–402.
[3] N. Kongsricharoern, C. Polprasert, Chromium removal by a bipolar electrochemical precipitation process, Water Sci. Technol., 34 (1996) 109–116.
[4] L. Monser, N. Adhoum, Modified activated carbon for the removal of copper zinc chromium and cyanide from wastewater, Sep. Purif. Technol., 26 (2002) 137–146.

[5] S. Rengaraj, K.H. Yeon, S.H. Moon, Removal of chromium from water and wastewater by ion exchange resins, J. Hazard. Mater., 87 (2001) 273–287.
[6] N. Ünlü, M. Ersoz, Adsorption characteristics of heavy metal ions onto a low cost biopolymeric sorbent from aqueous solutions, J. Hazard. Mater., 136 (2006) 272–280.
[7] V. Antochshuk, M. Jaroniec, 1-Allyl-3-propylthiourea modified mesoporous silica for mercury removal, Chem. Commun., 38 (2002) 258–259.
[8] M. Ghaedi, A.G. Nasab, S. Khodadoust, M. Rajabi, S. Azizian, Application of activated carbon as adsorbents for efficient removal of methylene blue: kinetics and equilibrium study, J. Ind. Eng. Chem., 20 (2014) 2317–2324.
[9] J.P. Zhao, W.C. Ren, H.M. Cheng, Graphene sponge for efficient and repeatable adsorption and desorption of water contaminations, J. Mater. Chem., 22 (2012) 20197–20202.
[10] X. Wang, J. Lu, B. Xing, Sorption of organic contaminants by carbon nanotubes: influence of adsorbed organic matter, Environ. Sci. Technol., 42 (2008) 3207–3212.
[11] Z.G. Pei, L.Y. Li, L.X. Sun, S.Z. Zhang, X.Q. Shan, S.Y. Yang, B. Wen, Adsorption characteristics of 1,2,4-trichlorobenzene, 2,4,6-trichlorophenol, 2-naphthol and naphthalene on graphene and graphene oxide, Carbon, 51 (2013) 156–163.
[12] K.S. Lin, H.W. Cheng, W.R. Chen, C.F. Wu, Synthesis, characterization, and adsorption kinetics of titania nanotubes for basic dye wastewater treatment, Adsorption, 16 (2010) 47–56.
[13] W. Gao, L.B. Alemany, L. Ci, P.M. Ajayan, New insights into the structure and reduction of graphite oxide, Nat. Chem., 1 (2009) 403–408.
[14] W.W. Cai, R.D. Piner, F.J. Stadermann, S. Park, M.A. Shaibat, Y. Ishii, D.X. Yang, A. Velamakanni, S.J. An, M. Stoller, J. An, D.M. Chen, R.S. Ruoff, Synthesis and solid-state NMR structural characterization of 13C-labeled graphite oxide, Science, 321 (2008) 1815–1817.
[15] V. Singh, D. Joung, L. Zhai, S. Das, S.I. Khondaker, S. Seal, Graphene based materials: past, present and future, Prog. Mater. Sci., 56 (2011) 1178–1271.
[16] Q. Li, Y.H. Li, X.M. Ma, Q.J. Du, K.Y. Sui, D.C. Wang, C.P. Wang, H.L. Li, Y.Z. Xia, Filtration and adsorption properties of porous calcium alginate membrane for methylene blue removal from water, Chem. Eng. J., 316 (2017) 623–630.
[17] Y. Liu, S. Chen, L. Zhong, G. Wu, Preparation of high-stable silver nanoparticle dispersion by using sodium alginate as a stabilizer under gamma radiation, Radiat. Phys. Chem., 78 (2009) 251–255.
[18] F. Zhao, E. Repo, D.L. Yin, Y. Meng, S. Jafari, M. Sillanpää, EDTA-cross-linked β-cyclodextrin: an environmentally friendly bifunctional adsorbent for simultaneous adsorption of metals and cationic dyes, Environ. Sci. Technol., 49 (2015) 10570–10580.
[19] D.C. Marcano, D.V. Kosynkin, J.M. Berlin, A. Sinitskii, Z.Z. Sun, A. Slesarev, B.A. Lawrence, W. Lu, J.M. Tour, Improved synthesis of graphene oxide, ACS Nano, 4 (2010) 4806–4814.
[20] Y. Zhang, F. Liang, W.W. Qiao, Z. Chen, M. Li, P.G. Dian, The synthesis of sodium alginate composites and their removal performances toward Pb^{2+} and Cd^{2+}, Desal. Water Treat., 158 (2019) 199–206.
[21] T.F. Huang, L. Zhang, H.L. Chen, C.J. Gao, Sol–gel fabrication of a non-laminated graphene oxide membrane for oil/water separation, J. Mater. Chem. A, 3 (2015) 19517–19524.
[22] M. Hu, B. Mi, Enabling graphene oxide nanosheets as water separation membranes, Environ. Sci. Technol., 47 (2013) 3715–3723.
[23] C.L. Jiao, P.G. Xiong, J. Tao, S.J. Xu, D.S. Zhang, H. Lin, Y.Y. Chen, Sodium alginate/graphene oxide aerogel with enhanced strength-toughness and its heavy metal adsorption study, Int. J. Biol. Macromol., 83 (2016) 133–141.
[24] W.C. Wan, Y.H. Lin, A. Prakash, Y. Zhou, Three-dimensional carbon-based architectures for oil remediation: from synthesis and modification to functionalization, J. Mater. Chem. A, 4 (2016) 18687–18705.
[25] H.C. Zheng, J.S. Yang, S.Y. Han, The synthesis and characteristics of sodium alginate/graphene oxide composite films crosslinked with multivalent cations, J. Appl. Polym. Sci., 133 (2016) 43616–43623.
[26] M. Rosa, J.M. Tiago, S.K. Singh, V. Geraldes, M.A. Rodrigues, Improving heat transfer at the bottom of vials for consistent freeze drying with unidirectional structured ice, AAPS PharmSciTech, 17 (2016) 1049–1059.
[27] K. Kim, Y. Oh, M.F. Islam, Graphene coating makes carbon nanotube aerogels superelastic and resistant to fatigue, Nat. Nanotechnol., 7 (2012) 562–566.
[28] Y.Q. Li, D.Y. Pan, S.B. Chen, Q.H. Wang, G.Q. Pan, T.M. Wang, *In situ* polymerization and mechanical, thermal properties of polyurethane/grapheme oxide/epoxy nanocomposites, Mater. Des., 47 (2013) 850–856.
[29] Y.X. Luo, A. Lode, C.T. Wu, J. Chang, M. Gelinsky, Alginate/nanohydroxyapatite scaffolds with designed core/shell structures fabricated by 3D plotting and *in situ* mineralization for bone tissue engineering, ACS Appl. Mater. Interfaces, 7 (2015) 6541–6549.
[30] J. Yu, H.T. Zhang, Y. Li, Q.F. Lu, Q.Z. Wang, W. Yang, Synthesis, characterization, and property testing of PGS/P(AMPS-co-AM) superabsorbent hydrogel initiated by glow-discharge electrolysis plasma, Colloid Polym. Sci., 2016 (294) 257–270.
[31] J. Liu, P. Li, H. Xiao, Y. Zhang, X. Shi, X. Lü, X. Chen, Understanding flocculation mechanism of graphene oxide for organic dyes from water: experimental and molecular dynamics simulation, AIP Adv., 5 (2015) 117151–117158.
[32] J.W. Li, J.M. He, Y.D. Huang, D.L. Li, X.T. Chen, Improving surface and mechanical properties of alginate films by using ethanol as a co-solvent during external gelation, Carbohydr. Polym., 123 (2015) 208–216.
[33] L. Liu, Y. Wan, Y. Xie, R. Zhai, B. Zhang, J. Liu, The removal of dye from aqueous solution using alginate-halloysite nanotube beads, Chem. Eng. J., 187 (2012) 210–216.
[34] R.A. Day, A.L. Underwood, Quantitative Analysis, 6th ed., Prentice Hall, New Delhi, India, 1993.
[35] P.S.S. Babu, Z. Khan, Electron transfer reaction in the chromium(VI)-manganese(II) system in the presence of ethylenediaminetetraacetic acid (EDTA), Transition Met. Chem., 29 (2004) 885–892.
[36] K.G. Sreejalekshmi, K.A. Krishnan, T.S. Anirudhan, Adsorption of Pb(II) and Pb(II)-citric acid on sawdust activated carbon: kinetic and equilibrium isotherm studies, J. Hazard. Mater., 161 (2009) 1506–1513.
[37] J. Yu, J.D. Zheng, Q.F. Lu, S.X. Yang, X.M. Zhang, X. Wang, W. Yang, Selective adsorption and reusability behavior for $Pb^{2+}$and Cd^{2+} on chitosan/poly(ethylene glycol)/poly(acrylic acid) adsorbent prepared by glow-discharge electrolysis plasma, Colloid Polym. Sci., 294 (2016) 1585–1598.
[38] X. Deng, L. Lu, H. Li, F. Luo, The adsorption properties of Pb(II) and Cd(II) on functionalized graphene prepared by electrolysis method, J. Hazard. Mater., 183 (2010) 923–930.
[39] G. Zhao, J. Li, X. Ren, C. Chen, X. Wang, Few-layered graphene oxide nanosheets as superior sorbents for heavy metal ion pollution management, Environ. Sci. Technol., 45 (2011) 10454–10462.
[40] Y. Yang, Y. Xie, L. Pang, M. Li, X. Song, J. Wen, H. Zhao, Preparation of reduced graphene oxide/poly(acrylamide) nanocomposite and its adsorption of Pb(II) and methylene blue, Langmuir, 29 (2013) 10727–10736.
[41] S. Sheshmani, M. Akhundi Nematzadeh, S. Shokrollahzadeh, A. Ashori, Preparation of grapheme oxide/chitosan/FeOOH nanocomposite for the removal of Pb(II) from aqueous solution, Int. J. Biol. Macromol., 80 (2015) 475–480.
[42] M.Y. Chang, R.S. Juang, Adsorption of tannic acid, humic acid, and dyes from water using the composite of chitosan and activated clay, J. Colloid Interface Sci., 278 (2004) 18–25.
[43] A.R. Cestari, E.F.S. Vieira, J.D.S. Matos, F.S.C. Anjos, Determination of kinetic parameters of Cu(II) interaction with chemically modified thin chitosan membranes, J. Colloid Interface Sci., 285 (2005) 288–295.
[44] M. Xu, Y.S. Zhang, Z.M. Zhang, Y.O. Shen, M.J. Zhao, G.T. Pan, Study on the adsorption of Ca^{2+}, Cd^{2+} and Pb^{2+} by magnetic

Fe_3O_4 yeast treated with EDTA dianhydride, Chem. Eng. J., 168 (2011) 737–745.
[45] I. Uzun, Kinetics of the adsorption of reactive dyes by chitosan, Dyes Pigm., 70 (2006) 76–83.
[46] H. Freundlich, Over the adsorption in solution, J. Phys. Chem., 57 (1906) 1100–1107.
[47] J. Wang, B.L. Chen, B.S. Xing, Wrinkles and folds of activated graphene nanosheets as fast and efficient adsorptive sites for hydrophobic organic contaminants, Environ. Sci. Technol., 50 (2016) 3798–3808.
[48] P. Tan, J. Sun, Y.Y. Hu, Z. Fang, Q. Bi, Y.C. Chen, J.H. Cheng, Adsorption of Cu^{2+}, Cd^{2+} and Ni^{2+} from aqueous single metal solutions on graphene oxide membranes, J. Hazard. Mater., 297 (2015) 251–260.
[49] Z.M. Gao, T.J. Bandosz, Z.B. Zhao, M. Han, J.S. Qiu, Investigation of factors affecting adsorption of transition metals on oxidized carbon nanotubes, J. Hazard. Mater., 167 (2009) 357–365.
[50] C. Liu, R. Bai, Q. San Ly, Selective removal of copper and lead ions by electronegativity, J. Am. Chem. Soc., 105 (1983) 7512–7516.
[51] C.K. Liu, R.B. Bai, Q.S. Ly, Selective removal of copper and lead ions by diethylenetriamine-functionalized adsorbent: behaviors and mechanisms, Water Res., 42 (2008) 1511–1522.
[52] P. Tan, Y. Hu, Q. Bi, Competitive adsorption of Cu^{2+}, Cd^{2+} and Ni^{2+} from an aqueous solution on graphene oxide membranes, Colloids Surf., A, 509 (2016) 56–64.
[53] K.J. Powell, L.D. Pettit, IUPAC Stability Consrants Database, Academic Software, Otley, York, UK, 1997.
[54] L.H. Pan, Z.Q. Wang, Q. Yang, R.Y. Huang, Efficient removal of lead, copper and cadmium ions from water by a porous calcium alginate/graphene oxide composite aerogel, Nanomaterials, 8 (2018) 957–972.
[55] Z. Ezzeddine, I. Batonneau-Gener, Y. Pouilloux, H. Hamad, Z. Saad, V. Kazpard, Divalent heavy metals adsorption onto different types of EDTA-modified mesoporous materials: effectiveness and complexation rate, Microporous Mesoporous Mater., 212 (2015) 125–136.
[56] I. Langmuir, The constitution and fundament properties of solids and liquids. Part 1. Solids, J. Am. Chem. Soc., 38 (1916) 2221–2295.
[57] H. Freundlich, Colloid and Capillary, E. P. Dutton and Co., New York, NY, 1928.
[58] R. Cheng, M. Kang, S.T. Zhuang, L. Shi, X. Zheng, J.L. Wang, Adsorption of Sr(II) from water by mercerized bacterial cellulose membrane modified with EDTA, J. Hazard. Mater., 364 (2019) 645–653.